European Radiology (2023) 33:8477–8487
https://doi.org/10.1007/s00330-023-09807-6

European Radiology
ESR EUROPEAN SOCIETY OF RADIOLOGY

CARDIAC

A deep learning method for the automated assessment of paradoxical pulsation after myocardial infarction using multicenter cardiac MRI data

Bing-Hua Chen[1] · Chong-Wen Wu[1] · Dong-Aolei An[1] · Ji-Lei Zhang[2] · Yi-Hong Zhang[2] · Ling-Zhan Yu[1] · Kennedy Watson[3] · Luke Wesemann[3] · Jiani Hu[3] · Wei-Bo Chen[2] · Jian-Rong Xu[1] · Lei Zhao[4] · ChaoLu Feng[5] · Meng Jiang[6] · Jun Pu[6] · Lian-Ming Wu[1]

Received: 30 August 2022 / Revised: 12 March 2023 / Accepted: 26 March 2023 / Published online: 30 June 2023

Abstract

Objective The current study aimed to explore a deep convolutional neural network (DCNN) model that integrates multidimensional CMR data to accurately identify LV paradoxical pulsation after reperfusion by primary percutaneous coronary intervention with isolated anterior infarction.

Methods A total of 401 participants (311 patients and 90 age-matched volunteers) were recruited for this prospective study. The two-dimensional UNet segmentation model of the LV and classification model for identifying paradoxical pulsation were established using the DCNN model. Features of 2- and 3-chamber images were extracted with 2-dimensional (2D) and 3D ResNets with masks generated by a segmentation model. Next, the accuracy of the segmentation model was evaluated using the Dice score and classification model by receiver operating characteristic (ROC) curve and confusion matrix. The areas under the ROC curve (AUCs) of the physicians in training and DCNN models were compared using the DeLong method.

Results The DCNN model showed that the AUCs for the detection of paradoxical pulsation were 0.97, 0.91, and 0.83 in the training, internal, and external testing cohorts, respectively ($p < 0.001$). The 2.5-dimensional model established using the end-systolic and end-diastolic images combined with 2-chamber and 3-chamber images was more efficient than the 3D model. The discrimination performance of the DCNN model was better than that of physicians in training ($p < 0.05$).

Conclusions Compared to the model trained by 2-chamber or 3-chamber images alone or 3D multiview, our 2.5D multiview model can combine the information of 2-chamber and 3-chamber more efficiently and obtain the highest diagnostic sensitivity.

Clinical relevance statement A deep convolutional neural network model that integrates 2-chamber and 3-chamber CMR images can identify LV paradoxical pulsation which correlates with LV thrombosis, heart failure, ventricular tachycardia after reperfusion by primary percutaneous coronary intervention with isolated anterior infarction.

Bing-Hua Chen, Chong-Wen Wu, Dong-Aolei An, ChaoLu Feng, Meng Jiang, Jun Pu, Lian-Ming Wu contributed equally to this work.

✉ ChaoLu Feng
fengchaolu@cse.neu.edu.cn

✉ Meng Jiang
jiangmeng0919@163.com

✉ Jun Pu
pujun310@hotmail.com

✉ Lian-Ming Wu
wlmssmu@126.com

[1] Department of Radiology, Renji Hospital, School of Medicine, Shanghai Jiao Tong University, No.160 PuJian Road, Shanghai 200127, China

[2] Philips Healthcare, Shanghai 201103, China

[3] Department of Radiology, Wayne State University, Detroit, MI 48201, USA

[4] Department of Radiololgy, Beijing Anzhen Hospital, Capital Medical University, Beijing 100029, China

[5] Key Laboratory of Intelligent Computing in Medical Image, Ministry of Education, No.195, Chuangxin Road, Hunnan District, Shenyang 110819, Liaoning, China

[6] Department of Cardiology, Renji Hospital, School of Medicine, Shanghai Jiao Tong University, No.160 PuJian Road, Shanghai 200127, China

Key Points

- *The epicardial segmentation model was established using the 2D UNet based on end-diastole 2- and 3-chamber cine images.*
- *The DCNN model proposed in this study had better performance for discriminating LV paradoxical pulsation accurately and objectively using CMR cine images after anterior AMI compared to the diagnosis of physicians in training.*
- *The 2.5-dimensional multiview model combined the information of 2- and 3-chamber efficiently and obtained the highest diagnostic sensitivity.*

Keywords Myocardial infarction · Magnetic resonance imaging · Ventricular remodeling · Deep learning

Abbreviations

2D UNet	Two-dimensional UNet
AMI	Acute myocardial infarction
BNP_{max}	Peak brain natriuretic peptide
$CK\text{-}MB_{max}$	Peak creatinine kinase-MB
CMR	Cardiac magnetic resonance
CRP_{max}	Peak C-creative protein
$cTnI_{max}$	Peak troponin I
DCNN	Deep convolutional neural network
HF	Heart failure
IMH	Intramyocardial hemorrhage
LAD	Left anterior descending
LGE	Late Gadolinium enhancement
LVEF	Left ventricular ejection fraction
LVT	Left ventricular thrombosis
MVO	Microvascular obstruction
NT-proBNP	N-terminal pro-brain natriuretic peptide
SSFP	Steady-state free-precession
T2WI-STIR	T2-weighted short-tau triple inversion recovery

Introduction

Following acute myocardial infarction, patients experience left ventricular dysfunction related to abnormal left ventricular wall motion. Due to the ongoing left ventricular remodeling, myocytes are lost while fibrosis increases within the infarct zone, which leads to further infarct expansion along with the volume expansion of the left ventricle [1, 2]. The paradoxical pulsation occurring during diastole and systole or only in systole patients after acute myocardial infarction (AMI) has been evaluated subjectively [3, 4]. Paradoxical pulsation is often complicated by left ventricular thrombosis (LVT), heart failure (HF), ventricular tachycardia, or angina after AMI. In a previous study, the incidence of left ventricular paradoxical pulsation was reported at 35% before thrombolysis [5], while morbidity was higher (39%) in patients with left anterior descending (LAD) culprit vessels based on angiocardiography [6]. Patients with complete occlusion of the proximal LAD coronary artery without collateral vessels might form left ventricle paradoxical pulsation [6]. The incidence of LVT in patients with paradoxical pulsation was reported at 26% [7]. Another critical intervention for paradoxical pulsation is the control of progressing HF due to deteriorating systolic dysfunction. Although left ventricular paradoxical pulsation has been reported since 1964 [8], the conventional assessment is based alone on visual interpretation of angiocardiography [5], echocardiography [9], or recently, cardiac magnetic resonance (CMR) imaging [4, 7]. However, visual interpretation is subjective and may significantly depend on personal experience. Thus, an accurate, effective, and objective method of analysis for the reduction of negligence and misinterpretation of left ventricular paradoxical pulsation is warranted.

CMR provides unique identification and prognostication of cardiovascular disease and has the advantages of non-ionizing radiation, a multiparametric approach, high-spatial/temporal resolution, and a non-invasive imaging modality. Deep learning methods based on CMR have become a robust intervention for analyzing and classifying cardiac diseases [10-16]. The deep learning algorithms can analyze multiparametric images of various CMR techniques [17, 18], which can delineate the location and morphology of LV paradoxical pulsation. Also, the results can be calculated directly without the step of predefined measurements as compared to the traditional machine learning algorithms [19]. The detailed information could then be extracted from CMR images with the deep layer of the convolutional neural network (DCNN) [10, 16], which in turn could accurately and effectively detect the abnormal movement and morphology of left ventricular paradoxical pulsation. Hypothetically, the DCNN trained with CMR images may provide automated and accurate detection of left ventricular paradoxical pulsation. The current study sought to explore a DCNN model which could automatically provide epicardial segmentation and discrimination of paradoxical pulsation among patients with isolated LAD culprit vessels using 2- and 3-chamber long-axis CMR cine images.

Materials and methods

Study population

A total of 401 participants were recruited to undergo CMR prospectively between September 2015 and October 2021 at the Shanghai Renji Hospital and Beijing Anzhen

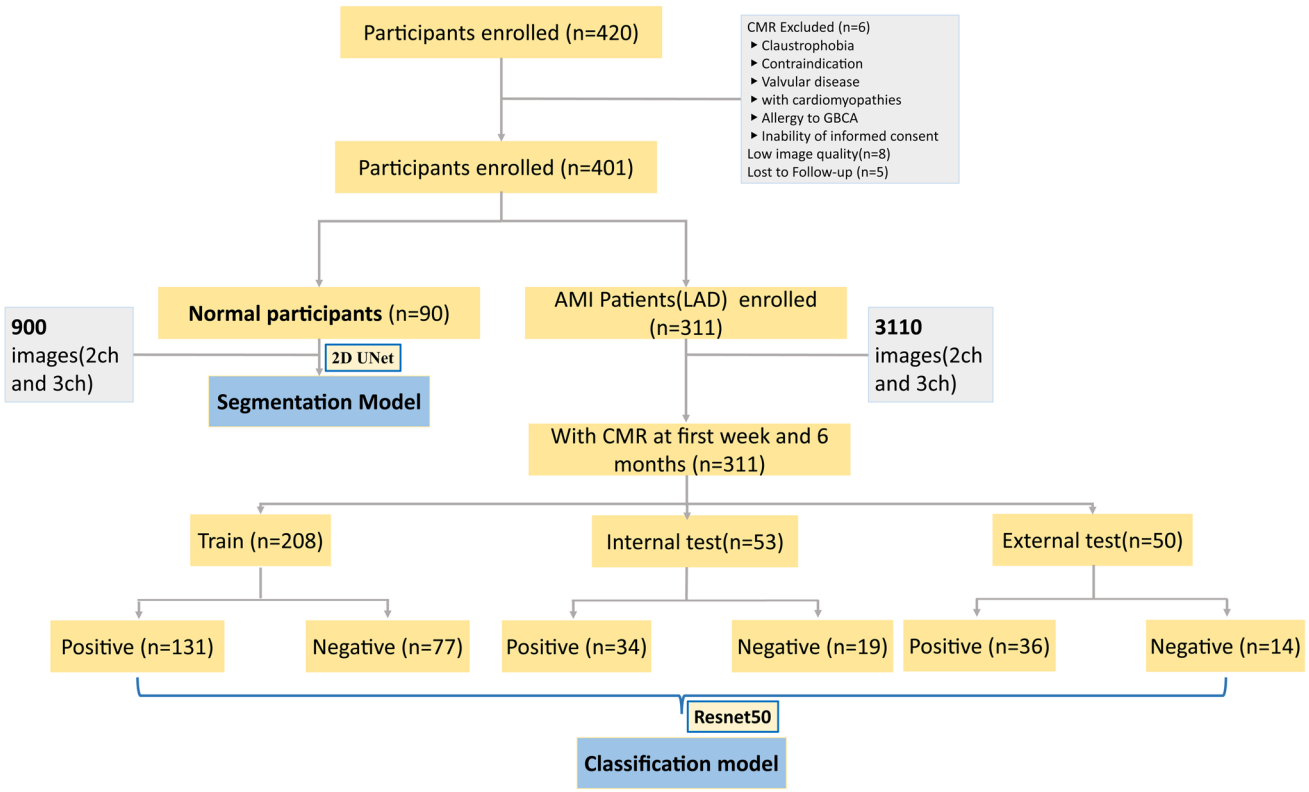

Fig. 1 Study flowchart. A total of 311 patients from multiple centers were divided into three groups: training group ($n=208$), internal test group ($n=53$), and external test group ($n=50$). Positive = with paradoxical pulsation, Negative = without paradoxical pulsation

Hospital, including 311 patients with anterior AMI and 90 age-matched normal volunteers. To overcome the issue of model generalizability, 311 patients from two centers were divided into three groups: training ($n=208$), internal test ($n=53$), and external test groups ($n=50$) (Fig. 1). AMI was diagnosed based on the standard definitions [20]. AMI patients with LAD culprit vessels who underwent primary percutaneous coronary intervention within 12 h of symptom onset were recruited in the current study. The inclusion and exclusion criteria are described in detail in the online *Appendix* (*Patient population*). The current CMR study protocol was approved by the institutional ethics committee and was conducted according to the Declaration of Helsinki. Written informed consent was obtained from all participants.

CMR imaging

All participants underwent CMR examinations within 1 week (median 3 days) after recruitment with a 3.0-T scanner (Ingenia, Philips Healthcare)**.** The CMR sequence parameters (T2WI-STIR, T2-weighted short-tau triple inversion recovery; SSFP, steady-state free-precession; T2* mapping; LGE, late gadolinium enhancement) are presented in Supplementary Table 1.

Analysis of CMR images

The diagnosis of LV paradoxical pulsation was based on the established definition of abnormal left ventricular wall motion [3, 21, 22]. The diagnosis of visual left ventricular paradoxical pulsation was made by a physician in training (A, with 3 years of experience, had diagnostic training before the project started) to compare with the accuracy of the DCNN model. The final diagnosis of left ventricular paradoxical pulsation was interpreted by the consensus of radiologists with at least 10 years of experience (experts B and C). The paradoxical pulsation mainly located in the anterior and anteroseptal wall could be well displayed in 2- and 3-chamber cine images and is manifested as the infarct zone outward protrusion in systole or both the systole and diastole [3, 21].

Deep learning models for epicardial segmentation and the prediction of paradoxical pulsation

Deep learning workflow

Cine MRI data standardization for deep learning models is presented in the *Supplementary file*. The deep learning framework consists of two stages (Fig. 2): (I) The epicardial segmentation model with 90 healthy volunteers was trained

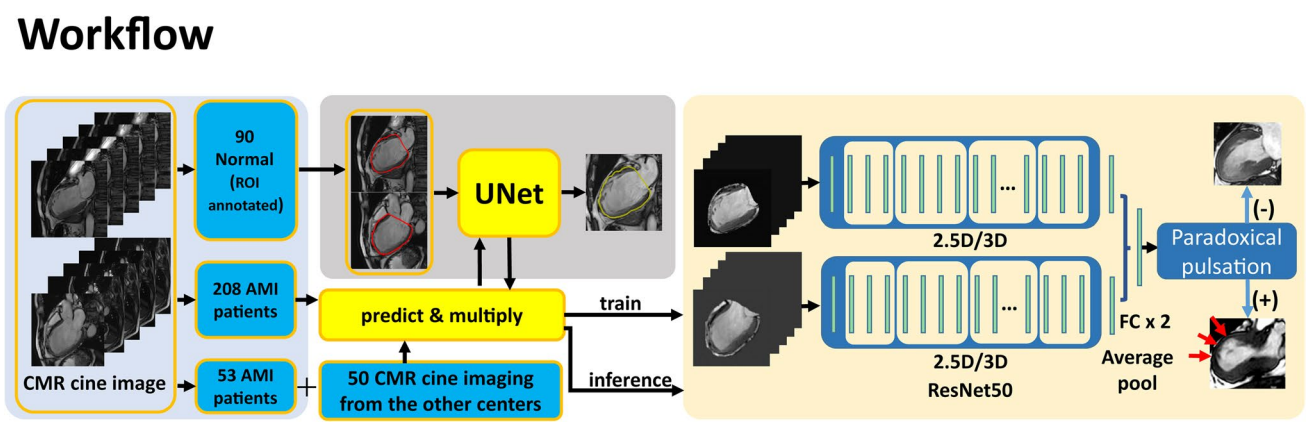

Fig. 2 Neural networks for the presence and region of paradoxical pulsation. The segmentation model was established using 90 healthy volunteers with both 2- and 3-chamber CMR cine images. The segmentation results of 208 AMI data predicted using the segmentation model were multiplied with the original image to train the classification model of paradoxical pulsation. The remaining 53 AMI data from our center and 50 data from another center were used as internal and external test cohorts, respectively, to evaluate the performance of the classification model

using 2D UNet based on end-diastole 2- and 3- chamber cine images. The detailed image processing and model structure were described in the *Image Annotation and Segmentation Model* of the *Supplementary file*. (II) The cine MRI data of 261 internal and 50 external patients with AMI were used to construct and evaluate a classification model for predicting the presence of left ventricular paradoxical pulsation. The contour of the epicardium as predicted by the segmentation model from step 1 was used as the mask and then multiplied by the normalized image as the input of the classification model.

Data preprocess

The data, including resampling, cropping, and normalization, are described in the *Cine MRI data standardization for deep learning models* section in the *Supplementary material.*

Segmentation model network

We delineated the epicardial contours of the 2- and 3-chambers for images of 90 volunteers without disease, and the data were used to establish a 2D segmentation model of the epicardial. The detailed process is described in the *Image Annotation and Segmentation Model* of the *Supplementary material.*

Classification model network

In order to eliminate the influence of background noise on the prediction model, the trained segmentation model was used to predict the epicardial mask of all heart phases of CMR cine data of AMI patients. The predicted epicardial mask was only allowed to retain the maximum connected area. Then, the median filter was used to filter the noise in the reserved area. The predicted masks were dilated by 11 pixels (11 mm) to ensure that the myocardium and blood pool were included. Finally, the predicted masks were used to multiply the normalized image. After eliminating the irrelevant tissues and background noise, the image was cropped to 200 × 200 pixels with the center point of the predicted epicardium. Subsequently, five images were selected at the end-systolic and end-diastolic phases as the input to train the classification model efficiently.

Inspired by breast cancer prediction in a previous study [23], we constructed a 2.5D multiview classification model, termed $\text{Model}_{\text{multi-view,}}$ based on Resnet50 [24] for the prediction of paradoxical pulsation after AMI. The architecture of $\text{Model}_{\text{multi-view}}$ is implemented, as shown in Fig. 2. Next, we retrained the ResNet50 to extract features from 2- and 3-chamber cine images. Since the input channel of our 2.5D model is 5, we applied the retrained model. Then, the features of the 2- and 3-chamber images were concatenated to obtain the prediction results through two fully connected layers.

CMR data of 261AMI patients were randomly split into 208 cases for training and validation and 53 cases in an independent test cohort, and 50 cases from another center comprised the external test cohort. The five-fold cross-validation of 208 cases included four-fold for training and one-fold for validation each time; finally, five models were established. Based on ensemble learning, the final result of each data was selected to average the results of five models. Adam (optimization algorithm) was used as the optimizer, cross-entropy was selected as the loss function, and the initial learning rate for network training was set to 0.001. If the validation loss did not decrease for 20 consecutive epochs, the learning rate decreased to half of the original, and if it did not decrease for 50 consecutive epochs, the training stopped.

Statistical analysis

Data analysis and evaluation metrics for deep learning models are presented in the *Supplementary file (Evaluation Metrics for deep learning models)*. The diagnostic

performance of a physician in training and our DCNN model was assessed using the receiver operating characteristic (ROC) curve analysis. The areas under the ROC curves (AUCs) of a physician in training and DCNN models were compared using the DeLong method. Statistical analysis was performed with Python (v3.7) with SciPy (v1.6.3), SPSS version 23.0 (IBM SPSS Inc.), and MedCalc version 11.4.2.0 (MedCalc Software). A two-tailed p value <0.05 was considered statistically significant.

Results

Study population

The cohort consisted of 401 participants with 4010 images, including 90 healthy controls for establishing the segmentation model and 311 patients for constructing the classification model. Patients with paradoxical pulsation displayed higher cardiac biomarkers ($cTnI_{max,}$ $CK\text{-}MB_{max}$, BNP_{max},

Table 1 Patient baseline characteristics

	Total ($n=311$)	Paradoxical pulsation (+) ($n=201$)	Paradoxical pulsation (-) ($n=110$)	p value
Age, yrs	54 (45, 63)	50 (40, 61)	57 (47, 64)	0.482
Female	17 (5.50%)	14 (7%)	3 (2.70%)	0.190
Body surface area, m^2	1.90 ± 0.17	1.86 ± 0.19	1.81 ± 0.14	0.020
Body mass index, kg/m^2	24.73 (23.29, 27.76)	27.55 (24.08, 29.58)	24.49 (22.99, 25.73)	0.268
Risk factors				
Hypertension	145 (46.62%)	91 (45.30%)	54 (49.10%)	0.519
Diabetes mellitus (II)	114 (36.66%)	80 (39.80%)	34 (30.90%)	0.120
$CK\text{-}MB_{max}$, U/L	169.50 (59, 284.35)	184.70 (88, 297.50)	125 (41.30, 207.80)	< 0.001
$cTnI_{max}$, ng/mL	26.50 (12.86, 31.70)	27.86 (16.77, 43.58)	17.52 (10.56, 30)	< 0.001
BNP_{max}, pg/mL	269.50 (133.75, 558)	345 (170.50, 615)	223 (108, 427)	< 0.001
$NT\text{-}proBNP_{max}$, pg/mL	1410 (844, 2679)	2032 (1400.50, 3050)	1016 (669, 1913.70)	< 0.001
CRP_{max}, mg/L	14.92 (7.55, 24)	19.73 (9.42, 54)	11.73 (3, 17.14)	< 0.001
Total cholesterol, mg/dL	4.40 (3.47, 5.27)	4.40 (3.47, 5.27)	4.40 (3.59, 5.23)	0.560
HDL	0.90 (0.80, 1.10)	0.88 (0.78, 1.07)	0.92 (0.82, 1.15)	0.489
Triglycerides, mg/dL	1.54 (1.07, 2.09)	1.64 (1.14, 2.09)	1.40 (1.01, 2.04)	0.263
CMR				
LVEDV, mL	160.52 ± 39.17	156.45 ± 40.31	133.54 ± 30.89	< 0.001
LVESV, mL	80.50 (61, 106)	106 (79.50, 127)	70 (49, 87.63)	< 0.001
SV, mL	77 (64, 86.53)	77 (66, 90.39)	76 (61.20, 86)	0.176
LV mass, g	125 (107, 147)	133 (113.56, 147)	116 (103, 134.30)	< 0.001
LVEDVi, mL/m^2	83.62 ± 17.31	83.81 ± 19.67	73.62 ± 15.58	< 0.001
LVESVi, mL/m^2	42.42 (31.99, 55.51)	51.44 (39.59, 61.41)	36.71 (27.47, 44.28)	< 0.001
SVi, mL/m^2	39.85 (34.84, 46.26)	38.65 (34.38, 44.33)	39.85 (35.07, 47.16)	0.001
LV massi, g/m^2	66.78 (58.04, 77.24)	67.76 (56.96, 71.81)	62.53 (56.29, 75.89)	0.001
LVEF, %	47.50 (40, 57)	43.90 (36, 51.30)	53.49 (45.39, 60)	< 0.001
LGE, %	28.39 (20.07, 37.32)	37 (28.80, 48.10)	21 (13, 26)	< 0.001
IMH	216 (69.45%)	168 (83.60%)	48 (43.60%)	< 0.001
MVO	214 (68.81%)	163 (81.10%)	51 (46.40%)	< 0.001
Transmural infarction	230 (73.95%)	184 (80%)	46 (20%)	< 0.001
Pericardial effusion	220 (70.74%)	159 (72.30%)	61 (27.70%)	< 0.001
LVT	101 (32.50%)	85 (42.30%)	16 (14.50%)	< 0.001
HF	93 (29.90%)	88 (43.80%)	5 (4.50%)	< 0.001

Numbers are given as median (inter-quartile ranges) or mean ± standard deviation or as the absolute frequency with percentages in parentheses. p value represents a comparison of patients with paradoxical pulsation and without paradoxical pulsation. *$cTnI_{max}$*, peak troponin I; *$CK\text{-}MB_{max}$*, peak creatinine kinase-MB; *BNP_{max}*, peak brain natriuretic peptide; *NT-proBNP*, N-terminal pro brain natriuretic peptide; *CRP_{max}*, peak c-creative protein; *MVO*, microvascular obstruction; *IMH*, intramyocardial hemorrhage; *LVEDV*, left ventricular end-diastolic volume; *LVESV*, left ventricular end-systolic volume; *SV*, stroke volume; *LVEF*, left ventricular ejection fraction; *LVEDVi*, indexed left ventricular end-diastolic volume; *LGE*, late gadolinium enhancement; *LVT*, left ventricular thrombosis; *HF*, heart failure

and NT-ProBNP$_{max}$) and inflammation (CRP$_{max}$) ($p < 0.001$) (Table 1). Patients with paradoxical pulsation might be accompanied by IMH, MVO, and pericardial effusion and manifested as transmural infarction ($p < 0.001$), had low LVEF and high LGE ($p < 0.001$), and were more likely to form mural thrombi in the LV than those without paradoxical pulsation (42.30% and 14.50%, $p < 0.001$). In the current study, 93/311 (29.90%) patients presented HF during follow-up. Patients with left ventricular paradoxical pulsation were more likely to progress to HF than those without the phenotype (43.80% *vs*. 4.50%, $p < 0.001$). Moreover, paradoxical pulsation was significantly correlated with HF ($r = 0.34$, $p < 0.001$).

Epicardial segmentation

In the epicardial segmentation model, the mean Dice scores of the training, validation, and test cohorts were 0.97, 0.96, and 0.96, respectively (Supplementary Fig. 1). In the test cohort, the lowest (0.94), middle (0.97), and highest Dice (0.98) scores were acquired. The segmentation with the lowest Dice could accurately identify the contour of the epicardium.

Classification model and validation of the DCNN model

Loss descent curve

Herein, we present a loss descent curve of validation and training data sets for training for onefold of the models in Fig. 3. Initially, the loss of both training and validation cohorts decreased. However, after 19 epochs, the loss of the training cohort reduced slowly, and the loss of the cohort did not decrease. According to our strategy, the model stopped training at the 69th epoch. The validation loss did not decrease again after 19 epochs. Hence, we selected the model at the 19th epoch with the minimum loss function of the validation as the final model to avoid overfitting.

Overall performance and discrimination of the models

The AUCs of the Model$_{multi\text{-}view}$ of the training cohort, internal test set, and external test set were 0.97 (0.94–0.99), 0.91 (0.80–0.97), and 0.83 (0.69–0.92), respectively ($p < 0.001$) (Table 2).

In addition to our model with multiple views, 2- and 3-chamber of data were trained independently with ResNet50, termed Model$_{2ch}$ and Model$_{3ch}$, respectively. The detailed results are shown in Table 2. The AUCs obtained by Model$_{2ch}$ alone were 0.97 (0.95–0.99), 0.89 (0.80–0.98), and 0.67 (0.52–0.82) on the training, internal, and external test cohorts, respectively, the AUCs obtained using the 3-chamber data were 0.99 (0.98–1.00), 0.89 (0.81–0.98), and 0.65 (0.48–0.83), respectively. Although the Model$_{2ch}$ or Model$_{3ch}$ could also achieve good results in the training cohort, the multiview model displayed better performance in the test cohort. Especially, on the external test set, the multiview model reached an AUC of 0.83 when that of the single-view model was ≤ 0.70. Model$_{multi\text{-}view}$ achieved the highest sensitivity in the test cohort, 0.88 and 0.89 in the internal and external test cohorts, respectively, which was much higher than the Model$_{2ch}$ and Model$_{3ch}$. This illustrated that the model combining 2-chamber and 3-chamber data was sensitive in discriminating the paradoxical pulsation and had a low rate of missed diagnosis, which was crucial for clinical diagnosis.

The current data are 3D, which recorded the cardiac structure and function over a period. Herein, we attempted to establish a 3D classification model called Model$_{multi\text{-}view\text{-}3D}$ to explore whether the model learning from the whole heart structure and function would have enhanced performance in paradoxical pulsation classification. The results are shown in Table 2. The AUCs for Model$_{multi\text{-}view\text{-}3D}$ were 0.99 (0.97–1.00), 0.87 (0.77–0.96), and 0.84 (0.74–0.95) in the training, internal, and external tests, which were not significantly different from the 2.5D model. Although the 3D model achieved the highest AUC on the external test set, its sensitivity to paradoxical pulsation was only 0.69, indicating that the model might have missed several patients with paradoxical pulsation.

While establishing Model$_{multi\text{-}view}$, the fixed heart phase was selected from the end-diastolic and end-systolic images.

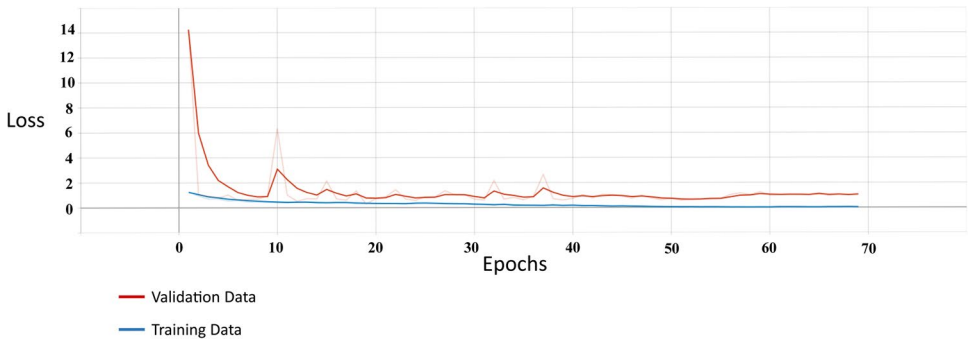

Fig. 3 The DCNN model converges in the process of the training. The value of the loss function decreased smoothly without large fluctuations in our validation and training data sets for training the best DCNN model

Table 2 Diagnostic performance for three datasets in five models

Model	Datasets	Cut-off	Accuracy	Sensitivity	Specificity	PPV	NPV	AUC	*p*
$Model_{multi\text{-}view}$	Train	0.46	0.92	0.93	0.90	0.94	0.89	0.97 (0.94 –0.99)	< 0.001
	Internal	0.43	0.85	0.88	0.79	0.88	0.79	0.91 (0.80 –0.97)	< 0.001
	External	0.29	0.84	0.89	0.71	0.89	0.71	0.83 (0.69 –0.92)	< 0.001
$Model_{2CH}$	Train	0.44	0.93	0.97	0.87	0.93	0.94	0.97 (0.95–0.99)	< 0.001
	Internal	0.49	0.83	0.77	0.95	0.96	0.69	0.89 (0.80–0.98)	< 0.001
	External	0.31	0.62	0.50	0.93	0.95	0.42	0.67 (0.52–0.82)	0.031
$Model_{3CH}$	Train	0.54	0.94	0.92	0.99	0.99	0.87	0.99 (0.98–1.00)	< 0.001
	Internal	0.62	0.77	0.65	1.00	1.00	0.61	0.89 (0.81–0.98)	< 0.001
	External	0.38	0.62	0.58	0.71	0.84	0.40	0.65 (0.48–0.83)	0.097
$Model_{multi\text{-}view\text{-}3D}$	Train	0.56	0.94	0.93	0.96	0.98	0.89	0.99 (0.97–1.00)	< 0.001
	Internal	0.37	0.83	0.94	0.63	0.82	0.86	0.87 (0.77–0.96)	< 0.001
	External	0.42	0.76	0.69	0.93	0.96	0.54	0.84 (0.74–0.95)	< 0.001
$Model_{multi\text{-}view\text{-}seg}$	Train	0.46	0.97	0.96	0.97	0.98	0.94	0.99 (0.99–1.00)	< 0.001
	Internal	0.46	0.91	0.88	0.95	0.97	0.82	0.94 (0.88–1.00)	< 0.001
	External	0.52	0.64	0.58	0.79	0.88	0.42	0.67 (0.49–0.85)	0.064
Physician	Internal	-	-	0.74	0.84	-	-	0.79 (0.66–0.89)	< 0.001
	External	-	-	0.58	0.86	-	-	0.72 (0.58–0.84)	< 0.001

PPV, positive predictive value; *NPV*, negative predictive value; *AUC*, area under the curve. Optimal cutoffs were selected using the Youden J-index

$Model_{multi\text{-}view}$, Model trained by the 2- and 3- chamber images multiplied by the corresponding epicardium mask predicted by the segmentation model

$Model_{2CH}$, Model trained by 2-chamber images multiplied by the corresponding epicardium mask

$Model_{3CH}$, Model trained by 3-chamber images multiplied by the corresponding epicardium mask

$Model_{multi\text{-}view\text{-}3D}$, Model trained by all the heart phases of the 2- and 3- chamber CMR images multiplied by the corresponding epicardium mask

$Model_{multi\text{-}view\_seg}$, Model trained by the 2- and 3- chamber images selected by mask multiplied by the corresponding epicardium mask

Since we had a segmentation model of the epicardium, the area of each heart phase could be calculated based on the segmentation results, and accurate end-diastolic and end-systolic images could be collected. Therefore, we re-selected 2.5D images for modeling based on the segmentation results, and the results of the $Model_{multi\text{-}view\text{-}seg}$ are shown in Table 2. After correcting the images, the model improved on all metrics in the training and internal test cohorts with respect to the accuracy, specificity, and PPV on the internal test, to >0.9. This phenomenon confirmed an effective way to establish the model with end-diastolic and end-systolic images. However, the general performance of the model in an external test might be attributed to the segmentation model trained only with the internal data. Moreover, some differences were noted in the sequence parameters between the external and internal data, which might affect the segmentation results in the external test cohort.

In summary, the 2.5D model established using end-systolic and end-diastolic images combined with 2-chamber and 3-chamber images was efficient in paradoxical pulsation recognition. The diagnostic performance of different models for paradoxical pulsation classification in the training, internal, and external cohorts was evaluated from the test set (Fig. 4).

The comparison of the discrimination performance between the DCNN model and physicians in training revealed that the AUC of the DCNN for detection of paradoxical pulsation (0.91 (0.80–0.97)) in the internal test was significantly higher than that of physicians in training during the internal test (0.79 (0.66–0.89)) ($p=0.001$), and was higher in the external test the AUC of DCNN (0.83 (0.69–0.92)) than that of physicians in training (0.72 (0.58–0.84)) ($p=0.039$) (Fig. 5).

Discussion

This multicenter cohort of consecutive patients with isolated LAD culprit lesions that underwent CMR provided the following findings: (1) The objective DCNN model established in the current study was much more accurate in discriminating paradoxical movement with CMR cine images after anterior AMI compared to the physicians in training; (2) Compared to the model trained by 2-chamber or 3-chamber images alone or 3D multiview, our 2.5D multiview model combined the information of 2- and 3-chamber efficiently and obtain the highest diagnostic sensitivity.

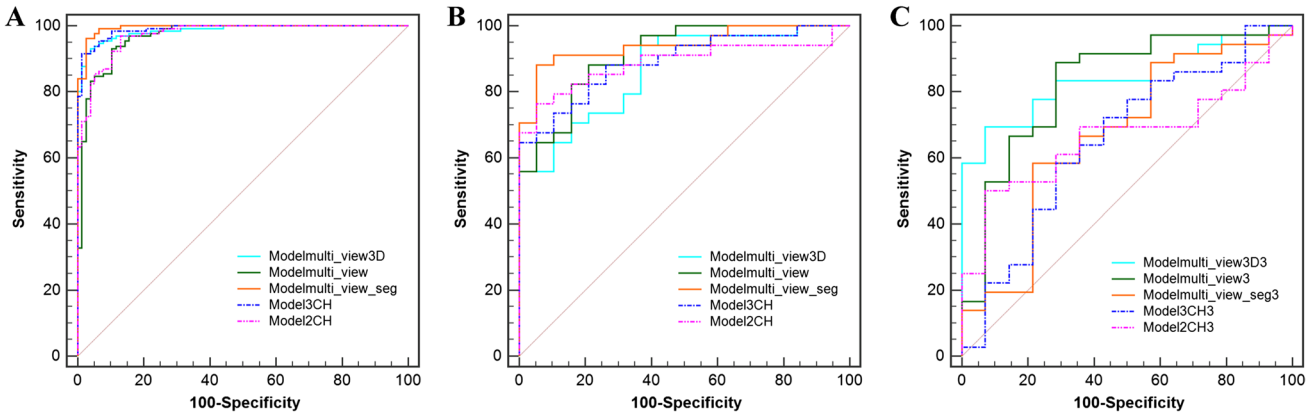

Fig. 4 **A** In the training set, the AUC of $Model_{multi\text{-}view}$ was lower than that of $Model_{multi\text{-}view\_seg}$ ($p=0.024$), the AUC of $Model_{multi\text{-}view}$ was lower than that of $model_{3ch}$ ($p=0.039$), and the AUC of $Model_{multi\text{-}view\_seg}$ was higher than that of $Model_{2ch}$ ($p=0.014$). **B** The differences among the models in the internal test were not significant. **C** In the external validation, the AUC of $Model_{multi\text{-}view}$ was higher than that of $Model_{multi\text{-}view\_seg}$ ($p=0.029$), the AUC of $Model_{multi\text{-}view}$ was higher than that of $model_{3ch}$ ($p=0.025$), and the AUC of $Model_{multiplied3D}$ was higher than that of $Model_{3ch}$ ($p=0.020$) and $Model_{2ch}$ ($p=0.004$)

Left ventricular paradoxical pulsation is defined as the left ventricular wall segments displaying paradoxical (dyskinetic) expansion at the systole and diastole or only at the systole [3, 21]. Mortality in the acute stage after AMI decreased over the past three decades; the main adverse impact was shifting from mortality to progressive left ventricular dysfunction and HF [25, 26]; the left ventricular paradoxical pulsation was significantly correlated with HF. Also, it is a manifestation of ventricular remodeling [27]. The left ventricle may undergo alterations in the structure, hemodynamics, and mechanics correlated to HF development and poor outcomes [28]. The increased wall stress in the remote myocardium may aggravate progressive LV dilation, eccentric hypertrophy, adverse remodeling, and HF [29, 30]. Both regional and global remodeling is correlated with the progression of paradoxical pulsation. Although global remodeling can be measured accurately, it is challenging to evaluate regional paradoxical pulsation.

The current study described an objective diagnostic model for LV paradoxical pulsation based on a deep learning algorithm. The DCNN model proposed in this study had better performance in discriminating paradoxical pulsation accurately and objectively with CMR cine images after AMI compared to physicians in training. Further improvements in the deep learning method may be achieved by the fusion of other imaging and clinical data. Thus, clinicians could further revise the diagnosis to improve the efficiency and accuracy based on the results of the DCNN model.

A previous study achieved accurate and fully automated CMR cine analysis on multivendor and multicenter data

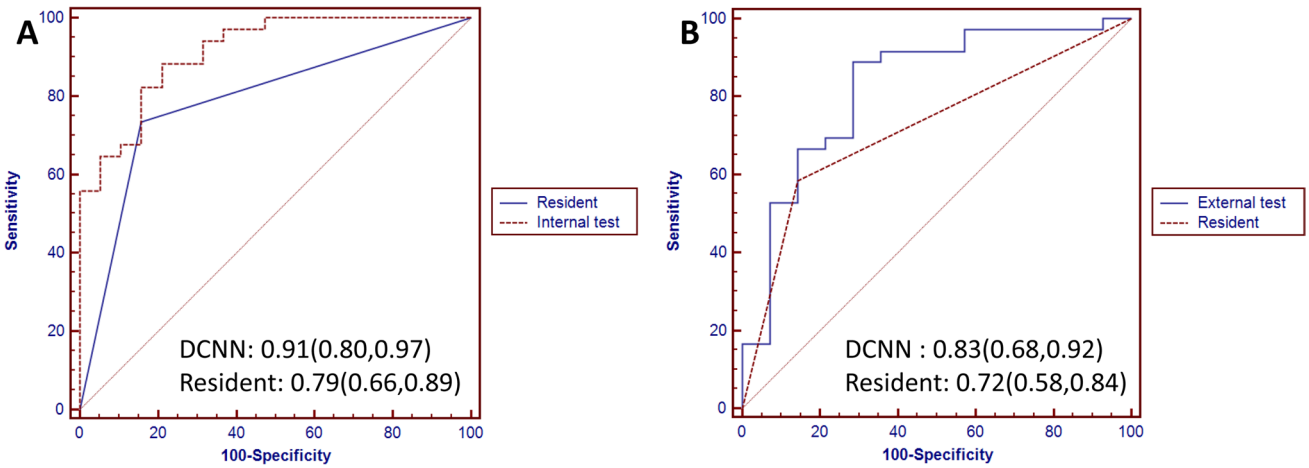

Fig. 5 AUCs for DCNN and physician in training. **A** The AUC of DCNN for the internal test set was higher than that of a physician in training (0.91 (0.80–0.97)) and (0.79 (0.66–0.89), $p=0.001$). **B** The AUC of DCNN for the external test set was higher than that of a physician in training (0.83 (0.68–0.92) and 0.72 (0.58–0.84), $p=0.039$)

based on the DCNN algorithm [31]. Some studies proposed a deep learning method on non-contrast CMR cine images that enabled rapid qualification and quantification of chronic myocardial infarction [32]. DCNN can be trained with an echocardiogram to characterize LV wall motion abnormalities [33] and can identify the extent of LV diastolic dysfunction to discriminate against patients with HF [34]. Left ventricular paradoxical pulsation in patients with acute anterior MI was located in the anterior and septal walls. The hybrid model was highly sensitive when combining the morphological information of long-axis 2- and 3-chamber CMR cine images. However, it may lead to misdiagnosis if based on the isolated 2- or 3-chamber. Nonetheless, models trained by 2- and 3-chamber images multiplied by the corresponding epicardial mask predicted by the segmentation model displayed the best performance compared to the isolated 2-chamber or 3-chamber images. The differences in AUC among the different models in the internal test cohort were not significant, while the mixed models were better than that model using isolated 2- or 3-chamber views in the external test cohort.

DCNN is the most common type of deep neural network for image postprocessing [16]. The epicardial segmentation model based on deep learning was constructed from the 2- and 3-chamber cine images of the healthy controls. The epicardial segmentation model is useful in extracting the morphological information of the whole heart. Herein, we applied the segmentation model of the epicardium to calculate the minimum and maximum epicardial area from the images as the input of the 2.5D model to correct our model ($Model_{multi\text{-}view\_seg}$). The differences between the AUC of the 2.5D and the 3D models were not significant, while the 3D model demonstrated lower sensitivity and required more storage space and longer processing time; the 2.5D model may be more efficient. Next, the segmentation contours were corrected manually to avoid the inaccurate segmentation of the external test cohort due to the different parameters of the CMR images between the two centers. The AUC of the training and internal test cohorts increased, while in the external test cohort, the result of $Model_{multi\text{-}view\_seg}$ decreased.

The classification performance was improved in the five models after being modified by the segmentation results of the external test cohort, although the differences were not significant. The training data of the segmentation model was small, with the possibility of overfitting. The model learned the noise of the internal data, leading to errors in the prediction of external data. Nonetheless, we could unify the distribution of the two data sets by histogram matching or add the training data of the segmentation model to overcome this deficiency. The results of the classification model suggested that the automated deep learning model can be used as a system to diagnose paradoxical pulsation and has a potential clinical value for the early detection of left ventricular paradoxical pulsation in AMI patients. This study also demonstrated the development of an automated and objective classification model for paradoxical pulsation based on a deep learning algorithm. The interpretation of paradoxical pulsation with CMR alone is observer-dependent and requires the experience of readers, while the deep learning algorithm is objective.

The outcomes of AMI patients with paradoxical pulsation remain controversial [5, 6, 35]. Paradoxical pulsation is associated with an adverse prognosis [5]. The paradoxical movement and progressive remodeling deteriorated the LV contractile function, thereby decreasing LVEF. Approximately 50% of patients with large or moderate paradoxical pulsation may have symptoms of HF [21]. Paradoxical pulsation can be complicated with HF, LVT, or ventricular tachycardia [36]. Systemic embolic events in patients with LVT and paradoxical pulsation tend to occur early after AMI. The early detection of paradoxical pulsation is critical for patients after AMI to achieve timely intervention.

Study limitations

Nevertheless, the current model has some limitations. Firstly, although we used data augmentation and early stopping to reduce overfitting in the modeling process, the small sample size for training and testing makes it challenging to highlight the performance improvements. However, in the current published studies, 311 patients with LAD culprit vessels underwent CMR imaging in acute and chronic stages. Secondly, the segmentation model is generated by a single-center training cohort, and there may be segmentation errors when applied to an external test cohort. The differences in the imaging parameters between the two hospitals are inevitable. Therefore, a larger and coincident data sample from multiple centers is essential to improve the DCNN model in future studies.

Conclusion

The DCNN model proposed in this study had better performance in discriminating left ventricular paradoxical pulsation accurately and objectively with CMR cine images after anterior AMI compared to the diagnosis of physicians in training. In addition, compared to the model trained by 2-chamber or 3-chamber images alone or 3D multiview, our 2.5D multiview model combined the information of 2-chamber and 3-chamber more efficiently and obtained the highest diagnostic sensitivity.

Supplementary Information The online version contains supplementary material available at https://doi.org/10.1007/s00330-023-09807-6.

Acknowledgements We are very grateful to the Philips Healthcare team for their support in image analysis and deep learning methods. We appreciate the support of Yan Zhou in providing a research platform

for this study. We appreciate Jun Pu and Meng Jiang made a great contribution to the study, mainly including patient recruitment, baseline clinical data collection, diagnosis, and standardized treatment.

Funding Supported by National Natural Science Foundation of China (No. 81873886, 81873887, and 82171884); National Natural Science Foundation of China Youth project (No. 82101981); Shanghai Science and Technology Innovation Action Plan, Technology Standard Project Grant numbers (No. 19DZ2203800); Shanghai Science and technology innovation action plan, technology standard project (No. 19DZ2203800); Shanghai Municipal Education Commission-Gaofeng Clinical Medicine Grant: Shanghai Jiao Tong University school of medicine Double hundred outstanding person project (No. 20191904); Shanghai Jiao Tong University Medical Engineering Cross Project (No. YG2022QN016).

Declarations

Guarantor The scientific guarantor of this publication is Lian-Ming Wu.

Conflict of interest The authors state that there neither exists a conflict of interest nor that there is financial information to disclose.

Statistics and biometry Lian-Ming Wu kindly provided statistical advice for this manuscript.

Informed consent Written informed consent was obtained from all participants in this study.

Ethical approval Institutional Review Board approval was obtained.

Study subjects or cohorts overlap Study subjects or cohorts have not been previously reported.

Methodology
- Prospective
- Observational
- Multicentre study

References

1. Kidambi A, Motwani M, Uddin A et al (2017) Myocardial extracellular volume estimation by CMR predicts functional recovery following acute MI. JACC Cardiovasc Imaging 10:989–999
2. D'Elia N, D'Hooge J, Marwick TH (2015) Association between myocardial mechanics and ischemic LV remodeling. JACC Cardiovasc Imaging 8:1430–1443
3. Cabin HS, Roberts WC (1980) Left ventricular aneurysm, intraaneurysmal thrombus and systemic embolus in coronary heart disease. Chest 77:586–590
4. Konen E, Merchant N, Gutierrez C et al (2005) True versus false left ventricular aneurysm: differentiation with MR imaging–initial experience. Radiology 236:65–70
5. Meizlish J, Berger H, Plankey M, Errico D, Levy W, Zaret B (1984) Functional left ventricular aneurysm formation after acute anterior transmural myocardial infarction. Incidence, natural history, and prognostic implications. N Engl J Med 311:1001–1006
6. Shen W, Tribouilloy C, Mirode A, Dufossé H, Lesbre J (1992) Left ventricular aneurysm and prognosis in patients with first acute transmural anterior myocardial infarction and isolated left anterior descending artery disease. Eur Heart J 13:39–44
7. Heatlie GJ, Mohiaddin R (2005) Left ventricular aneurysm: comprehensive assessment of morphology, structure and thrombus using cardiovascular magnetic resonance. Clin Radiol 60:687–692
8. Lam C, Gale H, Drake E (1964) Surgical treatment of left ventricular aneurysms. JAMA 187:1-3
9. Matsumoto M, Watanabe F, Goto A et al (1985) Left ventricular aneurysm and the prediction of left ventricular enlargement studied by two-dimensional echocardiography: quantitative assessment of aneurysm size in relation to clinical course. Circulation 72:280–286
10. Zhou H, Li L, Liu Z et al (2021) Deep learning algorithm to improve hypertrophic cardiomyopathy mutation prediction using cardiac cine images. Eur Radiol 31:3931–3940
11. Montalt-Tordera J, Quail M, Steeden JA, Muthurangu V (2021) Reducing contrast agent dose in cardiovascular MR angiography with deep learning. J Magn Reson Imaging 54:795–805
12. Hamilton JI, Currey D, Rajagopalan S, Seiberlich N (2021) Deep learning reconstruction for cardiac magnetic resonance fingerprinting T1 and T2 mapping. Magn Reson Med 85:2127–2135
13. Ghadimi S, Auger DA, Feng X et al (2021) Fully-automated global and segmental strain analysis of DENSE cardiovascular magnetic resonance using deep learning for segmentation and phase unwrapping. J Cardiovasc Magn Reson 23:20
14. Duan J, Bello G, Schlemper J et al (2019) Automatic 3D bi-ventricular segmentation of cardiac images by a shape-refined multi-task deep learning approach. IEEE Trans Med Imaging. https://doi.org/10.1109/TMI.2019.2894322
15. Litjens G, Ciompi F, Wolterink JM et al (2019) State-of-the-art deep learning in cardiovascular image analysis. JACC Cardiovasc Imaging 12:1549–1565
16. Chen C, Qin C, Qiu H et al (2020) Deep learning for cardiac image segmentation: a review. Front Cardiovasc Med 7:25
17. Martini N, Aimo A, Barison A et al (2020) Deep learning to diagnose cardiac amyloidosis from cardiovascular magnetic resonance. J Cardiovasc Magn Reson 22:84
18. Goldfarb JW, Craft J, Cao JJ (2019) Water-fat separation and parameter mapping in cardiac MRI via deep learning with a convolutional neural network. J Magn Reson Imaging. https://doi.org/10.1002/jmri.26658
19. LeCun Y, Bengio Y, Hinton G (2015) Deep learning. Nature 521:436–444
20. Thygesen K, Alpert JS, Jaffe AS et al (2018) Fourth universal definition of myocardial infarction (2018). J Am Coll Cardiol 72:2231–2264
21. Douglas PZ, Peter L, Robert OB, Douglas LM, Gordon FT, Eugene B (2018) Braunwald's heart disease: a textbook of cardiovascular medicine, 11th Edition. Elsevier, Canada. BMH Med J:3067–3069
22. Joyce E, Hoogslag GE, Leong DP et al (2014) Association between left ventricular global longitudinal strain and adverse left ventricular dilatation after ST-segment-elevation myocardial infarction. Circ Cardiovasc Imaging 7:74–81
23. Geras KJ, Wolfson S, Shen Y et al (2017) High-resolution breast cancer screening with multiview deep convolutional neural networks. arXiv preprint arXiv:1703.07047. https://arxiv.org/abs/1703.07047. Accessed 19 June 2023
24. Juarez-Orozco LE, Martinez-Manzanera O, van der Zant FM, Knol RJJ, Knuuti J (2020) Deep learning in quantitative PET myocardial perfusion imaging: a study on cardiovascular event prediction. JACC Cardiovasc Imaging 13:180–182
25. Mehta RH, Harjai KJ, Cox D et al (2003) Clinical and angiographic correlates and outcomes of suboptimal coronary flow inpatients with acute myocardial infarction undergoing primary percutaneous coronary intervention. J Am Coll Cardiol 42:1739–1746

26. Writing Group M, Mozaffarian D, Benjamin EJ et al (2016) Heart disease and stroke statistics-2016 update: a report from the American Heart Association. Circulation 133:e38-360
27. Gupta KB, Ratcliffe MB, Fallert MA, Edmunds LH Jr, Bogen DK (1994) Changes in passive mechanical stiffness of myocardial tissue with aneurysm formation. Circulation 89:2315–2326
28. Goldberg RJ, Konstam MA (1999) Assessing the population burden from heart failure: need for sentinel population-based surveillance systems. Arch Intern Med 159:15–17
29. Shah AM, Solomon SD (2010) A unified view of ventricular remodelling. Eur J Heart Fail 12:779–781
30. Pezel T, Viallon M, Croisille P et al (2021) Imaging Interstitial fibrosis, left ventricular remodeling, and function in stage A and B heart failure. JACC Cardiovasc Imaging 14:1038–1052
31. Tao Q, Yan W, Wang Y et al (2019) Deep learning-based method for fully automatic quantification of left ventricle function from cine mr images: a multivendor, multicenter study. Radiology 290:81–88
32. Zhang N, Yang G, Gao Z et al (2019) Deep learning for diagnosis of chronic myocardial infarction on nonenhanced cardiac Cine MRI. Radiology 291:606–617
33. Kusunose K, Abe T, Haga A et al (2020) A deep learning approach for assessment of regional wall motion abnormality from echocardiographic images. JACC Cardiovasc Imaging 13:374–381
34. Pandey A, Kagiyama N, Yanamala N et al (2021) Deep-Learning models for the echocardiographic assessment of diastolic dysfunction. JACC Cardiovasc Imaging 14:1887–1900
35. Heras M, Sanz G, Betriu A, Mont L, de Flores T, Navarro-López F (1990) Does left ventricular aneurysm influence survival after acute myocardial infarction? Eur Heart J 11:441–446
36. Gong FF, Vaitenas I, Malaisrie SC, Maganti K (2021) Mechanical complications of acute myocardial infarction: a review. JAMA Cardiol 6:341–349